frontiers | Frontiers in Plant Science

TYPE Original Research
PUBLISHED 07 September 2022
DOI 10.3389/fpls.2022.934736

OPEN ACCESS

EDITED BY
Roland Valcke,
University of Hasselt, Belgium

REVIEWED BY
Juan B. Arellano,
Spanish National Research Council (CSIC), Spain
Julian Eaton-Rye,
University of Otago, New Zealand

*CORRESPONDENCE
Hiroshi Ishikita
hiro@appchem.t.u-tokyo.ac.jp

SPECIALTY SECTION
This article was submitted to Plant Cell Biology, a section of the journal Frontiers in Plant Science

RECEIVED 03 May 2022
ACCEPTED 08 August 2022
PUBLISHED 07 September 2022

CITATION
Sugo Y and Ishikita H (2022) Proton-mediated photoprotection mechanism in photosystem II. *Front. Plant Sci.* 13:934736. doi: 10.3389/fpls.2022.934736

Proton-mediated photoprotection mechanism in photosystem II

Yu Sugo[1] and Hiroshi Ishikita[1,2]*

[1]Department of Applied Chemistry, The University of Tokyo, Tokyo, Japan, [2]Research Center for Advanced Science and Technology, The University of Tokyo, Tokyo, Japan

Photo-induced charge separation, which is terminated by electron transfer from the primary quinone Q_A to the secondary quinone Q_B, provides the driving force for O_2 evolution in photosystem II (PSII). However, the backward charge recombination using the same electron-transfer pathway leads to the triplet chlorophyll formation, generating harmful singlet-oxygen species. Here, we investigated the molecular mechanism of proton-mediated $Q_A^{\cdot -}$ stabilization. Quantum mechanical/molecular mechanical (QM/MM) calculations show that in response to the loss of the bicarbonate ligand, a low-barrier H-bond forms between D2-His214 and $Q_A^{\cdot -}$. The migration of the proton from D2-His214 toward $Q_A^{\cdot -}$ stabilizes $Q_A^{\cdot -}$. The release of the bicarbonate ligand from the binding Fe^{2+} site is an energetically uphill process, whereas the bidentate-to-monodentate reorientation is almost isoenergetic. These suggest that the bicarbonate protonation and decomposition may be a basis of the mechanism of photoprotection *via* $Q_A^{\cdot -}/Q_AH^{\cdot}$ stabilization, increasing the Q_A redox potential and activating a charge-recombination pathway that does not generate the harmful singlet oxygen.

KEYWORDS

photoprotection, photoinhibition, low-barrier hydrogen bond (LBHB), bicarbonate, proton-coupled electron transfer (PCET), formate, D1-Tyr246, Q_BH_2 release/exchange

Introduction

The driving force for photosynthetic O_2 evolution is provided by the photo-induced charge separation at the reaction center of photosystem II (PSII). The electronic excitation of the chlorophyll leads to electron transfer *via* pheophytin in the D1 protein, $Pheo_{D1}$, to two plastoquinone molecules, Q_A and Q_B (Shen, 2015). The terminal electron acceptor Q_B accepts two electrons *via* the primary quinone Q_A and two protons. The non-heme Fe^{2+} complex, which comprises D1-His215, D2-His214, D1-His272, D2-His268, and bicarbonate (HCO_3^-), is equidistant from Q_A and Q_B (Shevela et al., 2012; **Figure 1A**). The bidentate bicarbonate is modeled in the majority of the reported PSII structures (e.g., Umena et al., 2011; Gisriel et al., 2022; **Figure 1A**), whereas not only the bidentate but also monodentate bicarbonate is modeled in the PsbM-deleted PSII

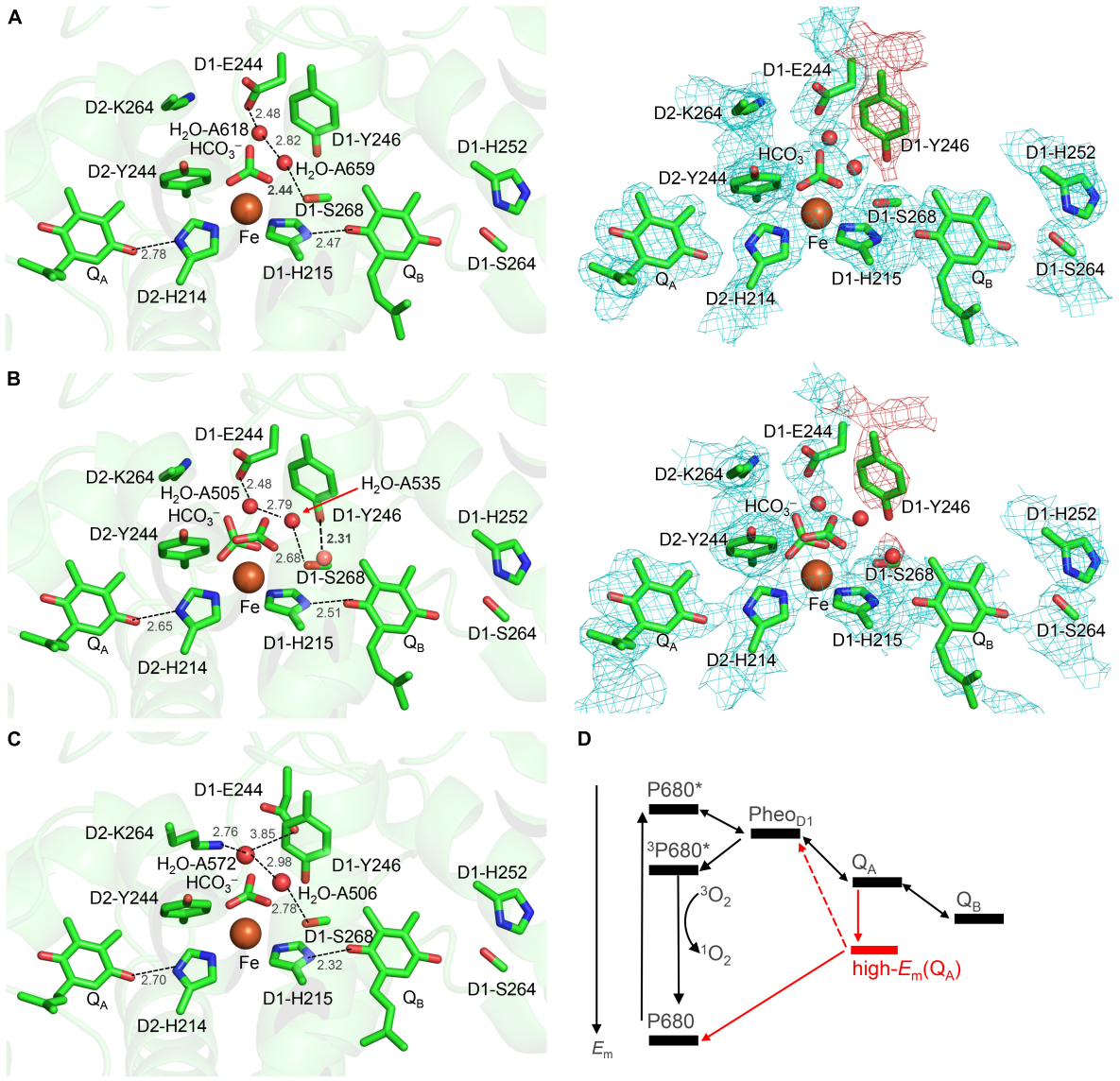

FIGURE 1
Overview of the quinone binding sites. **(A)** X-ray crystal structure of PSII from *Thermosynechococcus vulcanus* (PDB code, 3WU2) (Umena et al., 2011) and electron density map. **(B)** X-ray crystal structure of the PsbM-deleted PSII from *Thermosynechococcus vestitus* BP-1 (PDB code, 5H2F) (Uto et al., 2017) and electron density map. **(C)** Cryo-electron microscopy structure of PSII from *Synechocystis* sp. PCC 6803 (PDB code, 7N8O) (Ferreira et al., 2004). Dotted lines indicate H-bonds. The density of the D1-Tyr246 moiety, including the adjacent water molecule in the PsbM-deleted structure, is indicated by the red mesh. **(D)** Energetics of forward and backward electron-transfer processes. Processes occurring *via* the high-E_m Q_A form are shown in red. P680* denotes the electronically excited P680.

(**Figure 1B**; Uto et al., 2017). D1-Tyr246 and D2-Tyr244 are located at the bicarbonate binding site (Forsman et al., 2019). The characteristic of D1-Tyr246 is the electron density near the hydroxyl group (Saito et al., 2013), which is clearly observed in the 1.9-Å X-ray diffraction (XRD) (Umena et al., 2011) and X-ray free electron laser (XFEL)-S_1 (Suga et al., 2015) structures (**Figure 1A**). The experimentally observed electron density was not interpreted in 2011 and 2015 (**Figure 1A**). In 2017, Uto et al. (2017) modeled the corresponding density as a water molecule (*B*-factor: 40 Å^2) forming a significantly short H-bond with the hydroxyl group of D1-Tyr246 (2.31 Å) (**Figure 1B**). Remarkably, the $O_{D1-Tyr246}\ldots O_{water}$ distance of 2.3 Å is closer to the O…O distance for a typical Zundel ($H_2O\ldots H^+\ldots H_2O$) cation (≈2.3 Å). The absence of the corresponding density at the D2-Tyr244 moiety may indicate a functional asymmetry between the Q_A and Q_B sides (Saito et al., 2013).

The redox potential (E_m) values of −100 to −140 mV for one-electron reduction of Q_A ($Q_A/Q_A^{\cdot-}$) (Krieger and Weis, 1992; Johnson et al., 1995; Krieger et al., 1995; Ishikita and Knapp, 2005a; Shibamoto et al., 2009) and 90 mV for $Q_B/Q_B^{\cdot-}$

(Kato et al., 2016; De Causmaecker et al., 2019) indicate that exergonic electron transfer occurs under normal functional conditions. Reduced Q_B accepts the first proton *via* D1-Ser264 and D1-His252 at the distal carbonyl O site with respect to the non-heme Fe^{2+} complex (Ishikita and Knapp, 2005a; Saito et al., 2013; Ashizawa and Noguchi, 2014) and the second proton *via* D1-His215 at the proximal carbonyl O site (Saito et al., 2013, 2020; Kimura et al., 2020); thus, reduced Q_B forms Q_BH_2 and moves from PSII toward the quinone pool. The depletion of the bicarbonate from the non-heme Fe^{2+} reduces the rate of the electron transfer from Q_A to Q_B (Jursinic et al., 1976; Eaton-Rye and Govindjee, 1988) or the exchange of Q_BH_2 (Siggel et al., 1977; Sedoud et al., 2011).

Under strong light, the plastoquinone pool is fully reduced, and the Q_B binding site is unoccupied, which inhibits electron transfer and causes $Q_A^{\cdot -}$ to accumulate in PSII (photoinhibition) (Vass et al., 1992; Noguchi, 2002). If the E_m gap between Q_A and $Pheo_{D1}$ is small, backward electron transfer occurs in the form of charge recombination from $Q_A^{\cdot -}$ *via* $Pheo_{D1}$ to the cationic chlorophyll in the reaction center, forming triplet chlorophyll and generating harmful singlet-oxygen species (Rutherford and Krieger-Liszkay, 2001; Rutherford et al., 2012). Q_A has been reported to exhibit two forms, a low- and a high-$E_m(Q_A)$ conformation (**Figure 1D**; Krieger and Weis, 1992; Johnson et al., 1995; Krieger et al., 1995). Q_A exists in the low-potential form under normal functional conditions. The high-$E_m(Q_A)$ conformation can increase the E_m gap between Q_A and $Pheo_{D1}$, preventing charge recombination *via* $Pheo_{D1}$ and singlet-oxygen generation under strong light [photoprotection (Rutherford and Krieger-Liszkay, 2001; Rutherford et al., 2012)].

The molecular origin of the high-$E_m(Q_A)$ form had long remained unsolved. Vass et al. (1992) proposed that the $Q_A^{\cdot -}$ stabilization is mediated by protonation. In the 3.5-Å crystal structure of PSII (Ferreira et al., 2004), the OH group of D2-Thr217 forms an H-bond with $Q_A^{\cdot -}$ but not with unprotonated neutral Q_A (Ishikita and Knapp, 2005a). Thus, H-bond donation of D2-Thr217 to $Q_A^{\cdot -}$ could be a possible mechanism for the formation of the high-E_m conformation. However, the corresponding H-bond is unlikely to form in the crystal structure of PSII from *Thermosynechococcus vulcanus* (Umena et al., 2011) and the recent cryo-electron microscopy structure of PSII from *Synechocystis* sp. PCC 6803 (Gisriel et al., 2022). The aforementioned crystal structure shows that Q_A has D2-His214 at the proximal carbonyl O site and the backbone amide group of D2-Phe261 at the distal carbonyl O site as H-bond partners.

The non-heme Fe^{2+} complex might be involved in the photoprotection mechanism (Diner and Petrouleas, 1987; Muh et al., 2012). Notably, Brinkert et al. (2016) reported that the loss of the bicarbonate ligand from the non-heme Fe^{2+} complex leads to an increase of 75 mV in $E_m(Q_A)$ in the presence of Q_B; this suggests that the loss of the bicarbonate ligand is responsible for the formation of the high-$E_m(Q_A)$ conformation. Recent studies have shown that photo-induced CO_2 conversion is likely to occur from the bicarbonate ligand at Fe^{2+} (Shevela et al., 2020). Bicarbonate loss and photo-induced CO_2 conversion likely constitute the basis of the photoprotection mechanism. Although the loss of the negatively charged bicarbonate (HCO_3^-) certainly increases $E_m(Q_A)$, the distance between the bicarbonate ligand and Q_A is more than 6 Å (Umena et al., 2011). Moreover, whether the proton-mediated $Q_A^{\cdot -}$ stabilization mechanism (Vass et al., 1992) is still relevant to the $Q_A^{\cdot -}$ stabilization remains unclear.

To understand the mechanism of how the loss of the bicarbonate increases $E_m(Q_A)$, we investigated the bicarbonate and Q_A binding sites in PSII using a quantum mechanical/molecular mechanical (QM/MM) approach based on the PSII crystal structure (Umena et al., 2011).

Materials and methods

Coordinates and atomic partial charges

The atomic coordinates were obtained from the X-ray crystal structure of PSII (PDB code, 3WU2) (Umena et al., 2011). The heavy-atom positions were fixed while the H-atom positions were optimized with CHARMM (Brooks et al., 1983). All titratable groups were ionized if not otherwise specified. D1-His337 was considered to be protonated (Nakamura and Noguchi, 2017). Atomic partial charges were obtained from the CHARMM22 (MacKerell et al., 1998) parameter set for amino acids and previous studies for cofactors (Saito et al., 2015), respectively.

Quantum mechanical/molecular mechanical calculations

The unrestricted density functional theory method was employed with the B3LYP functional and LACVP* basis sets (LANL2DZ (double ζ quality basis set with the Los Alamos effective core potential) for Mn and Ca atoms and 6-31G* for other atoms) (Hay and Wadt, 1985) using the QSite (QSite, 2012) program. Counter ions were added to neutralize the system. In the QM region, all atomic coordinates were relaxed. In the MM region, the H-atom positions were energetically optimized, and the heavy-atom positions were fixed using the OPLS2005 force field because the MM region is used mainly to reproduce (long-distance) electrostatic interactions with the QM region and the heavy-atom positions in the MM region should remain unchanged with respect to those in the original crystal structure. The initial-guess wave functions were obtained using the ligand field theory (Vacek et al., 1999) implemented in the QSite program. Three QM regions were used: (i) [Q_A, Q_B, the non-heme Fe complex (bicarbonate if applicable, Fe,

and side chains of D1-His215, D1-His272, D2-His214, and D2-His268), side chains of D1-His252, D1-Ser264, and D2-Phe261 (including backbone)] for the analysis of the H-bond between Q_A and D2-His214; (ii) [Q_A, $Q_{B,}$ the non-heme Fe complex (bicarbonate, Fe, and side chains of D1-His215, D1-His272, D2-His214, and D2-His268), side chains of D1-Tyr246, D1-Ser264, and D1-His252, and the modeled water molecule adjacent to D1-Tyr246] for the analysis of the proton transfer toward the bicarbonate ligand; and (iii) [Q_A, $Q_{B,}$ the non-heme Fe complex (bicarbonate, Fe, and side chains of D1-His215, D1-His272, D2-His214, and D2-His268), side chains of D1-Tyr246, D1-Ser264, D1-His252, and protonated D1-Glu244, and water molecules in the H-bond network (water molecules A618 and A659 and the modeled water molecule adjacent to D1-Tyr246] for the analysis of the proton transfer from D1-Ser268 to the bicarbonate ligand.

All other protein units and cofactors were approximated by the MM force field (i.e., electrostatic influences are sufficiently considered in the MM region). Note that the residues in the proton transfer pathways must be included in the QM region to consider the formation/breakage of the covalent (H-)bonds during proton transfer. See **Supplementary material** for the atomic coordinates of the resulting QM region. As in a previous study (Chernev et al., 2011), the non-heme Fe complex was in a high-spin state of Fe^{2+}, and the spin multiplicity of the system was set to $S = 2$ in calculations for neutral Q_A and $S = 5/2$ for $Q_A^{\bullet-}$.

The QM/MM-optimized geometry was used as the initial geometry to analyze the potential energy profiles. For the analysis of the $N_{D2-His214}...H^+...O_{QA}$ H-bond, the focusing H atom was moved along the N...O H-bond from 0.02 to 0.10 Å (e.g., 0.02 Å around the local energy minimum in some

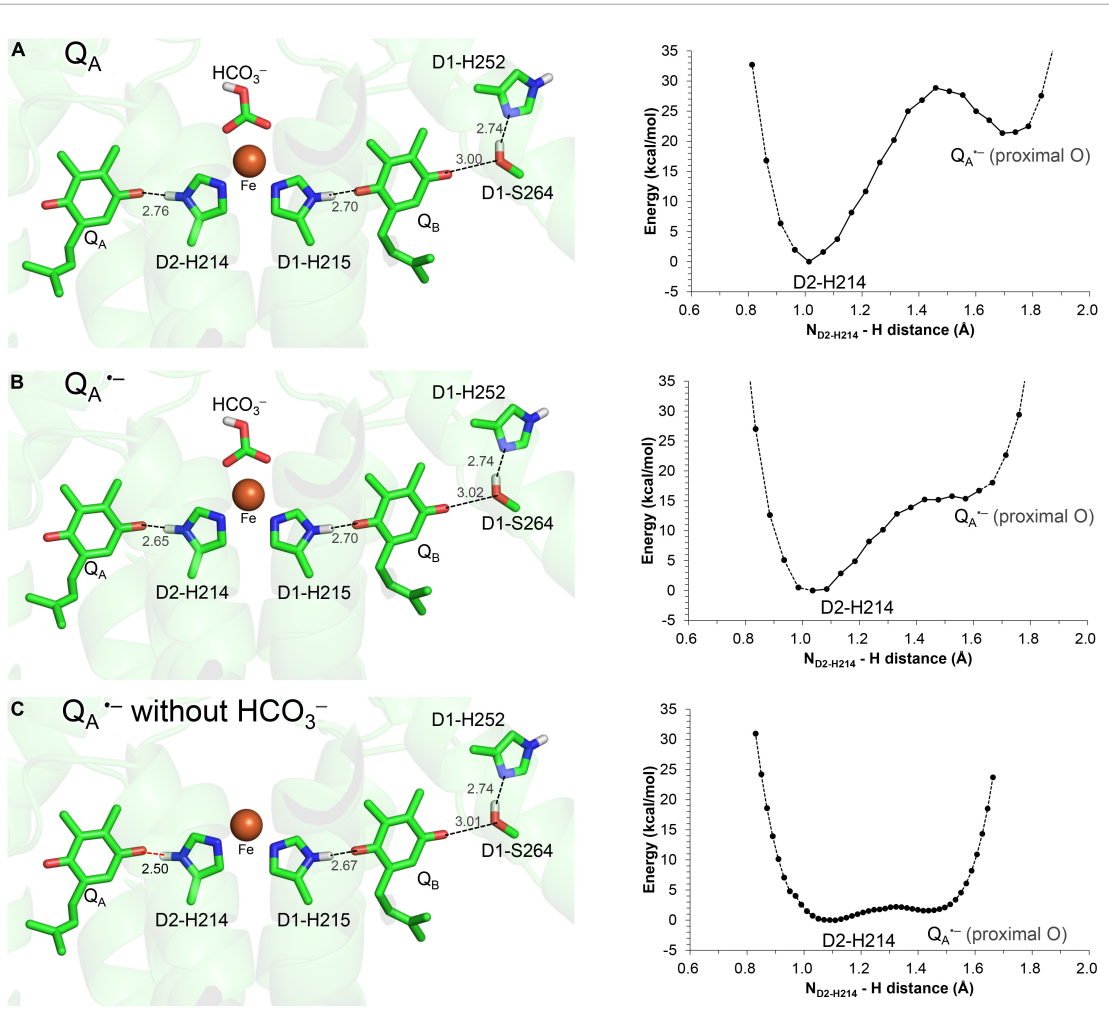

FIGURE 2
QM/MM-optimized geometry and potential energy profile for the H-bond between Q_A and D2-His214 prior to electron transfer from Q_A to Q_B. **(A)** Neutral Q_A. **(B)** $Q_A^{\bullet-}$. **(C)** $Q_A^{\bullet-}$ in the absence of the bicarbonate ligand. D1-Ser264 forms an H-bond with unprotonated D1-His252, as the electron is not transferred to Q_B (Ishikita and Knapp, 2005a). Note that the geometry of each intermediate conformation is fully QM/MM optimized.

cases), after which the geometry was optimized by constraining the N...H^+ and H^+...O distances and energy was calculated. For the analysis of the bidentate-to-monodentate reorientation of the bicarbonate ligand, the focusing O_{HCO3-}...Fe distance was increased by 0.10 Å, after which the geometry was optimized by constraining the O_{HCO3-}...Fe distance and energy was calculated. For the analysis of the release of the bicarbonate ligand from the Fe site, the C_{HCO3-}...Fe distance was increased by 0.10 Å, after which the geometry was optimized by constraining the C_{HCO3-}...Fe distance and energy was calculated. For the analysis of the proton transfer from H_3O^+ *via* D1-Tyr246 and the bicarbonate ligand, the focusing H atom was moved away from the electron donor O site from 0.02 to 0.10 Å, after which the geometry was optimized by constraining the O_{donor}...H distance and energy was calculated. For the analysis of the proton transfer from H_3O^+ adjacent to D1-Ser268 to the bicarbonate ligand, the focusing H atom was moved to the electron acceptor O site by 0.10 Å, after which the geometry was optimized by constraining the $O_{acceptor}$...H distance and energy was calculated. For the analysis of the protonated bicarbonate decomposition to H_2O + CO_2, the H_2O...CO_2 distance was increased by 0.10 Å, after which the geometry was optimized by constraining the H_2O...CO_2 distance and the energy was calculated.

Results

Formation of a low-barrier H-bond between D2-His214 and Q_A upon bicarbonate loss

The H-bond distance of 2.78 Å between D2-His214 and Q_A in the PSII crystal structure (Umena et al., 2011; **Figure 1A**) is closest to 2.76 Å for neutral unprotonated Q_A in the QM/MM-optimized geometry (**Figure 2A**). This suggests that Q_A is neutral Q_A in the PSII crystal structure. Although the H-bond is shortened to 2.65 Å when Q_A is reduced to $Q_A^{\cdot-}$, the potential-energy profile indicates that the H^+ is localized at the D2-His214 moiety (**Figure 2B**).

Remarkably, the D2-His214...$Q_A^{\cdot-}$ H-bond transforms into a low-barrier H-bond (2.50 Å) in response to the loss of the bicarbonate ligand (**Figure 2C**). In addition to the electrostatic contribution of the loss of the negative charge to an increase in $E_m(Q_A)$, the migration of the D2-His214 proton toward $Q_A^{\cdot-}$ along the low-barrier H-bond (0.23 Å) stabilizes $Q_A^{\cdot-}$ significantly. In addition to the loss of a negative charge, this is likely a substantial reason for the 75 mV upshift in $E_m(Q_A)$ upon the loss of the bicarbonate (Brinkert et al., 2016) because Q_A...HCO_3^- is not short (6.8 Å).

The formation of the low-barrier H-bond between $Q_A^{\cdot-}$ and D2-His214 suggests that $pK_a(Q_A^{\cdot-}/Q_AH) \approx pK_a$(D2-His214-NH/$N^-$) in the absence of the bicarbonate. The low-barrier H-bond formation is also observed between D1-His215 and Q_BH^- in PSII (Saito et al., 2013) [and His-L190 and Q_BH^- in photosynthetic reaction centers from purple bacteria (PbRC) (Sugo et al., 2021)] during the Q_BH_2 formation; this suggests that $pK_a(Q_BH^-/Q_BH_2) \approx pK_a$(D1-His215-NH/$N^-$) in the presence of the bicarbonate. pK_a(D1-His215-NH/N^-) and pK_a(D2-His214-NH/N^-) for deprotonation of singly protonated to anionic histidine are likely higher [e.g., 13 in the Rieske cluster (Zu et al., 2003; Hsueh et al., 2010)] than pK_a for deprotonation of doubly protonated to singly protonated histidine [e.g., 2–9 in protein environments (Grimsley et al., 2009)]. As $pK_a(QH^-/QH_2) = 11$ for plastoquinone (Q) in water (Hasegawa et al., 2017), a slight decrease in pK_a(D2-His214-NH/N^-) due to Fe^{2+} can lead to $pK_a(Q_a^{\cdot-}/Q_AH) \approx pK_a$(D2-His214-NH/$N^-$).

In the low-barrier H-bond, the proton can move easily between the two H-bond moieties (Ishikita and Saito, 2014). In the low-barrier H-bond between TyrZ and D1-His190, the 0.35 Å migration of the proton toward TyrZ from D1-His190 can increase E_m(TyrZ) by 130 mV (Saito et al., 2020). From the analogy, the > 0.2 Å migration of the proton toward $Q_A^{\cdot-}$ along the low-barrier H-bond (**Figure 2C**) is the most likely origin of the observed increase of 75 mV in $E_m(Q_A)$ (Brinkert et al., 2016). Thus, $Q_A^{\cdot-}$ can be stabilized irrespective of Q_A...HCO_3^- = 6.8 Å.

Energetics of the bicarbonate displacement from the non-heme Fe complex

In QM/MM calculations, the release of the bicarbonate ligand from the binding Fe^{2+} site is an energetically uphill process (**Figure 3A**), which suggests that the electrostatic interaction between Fe^{2+} and HCO_3^- is not negligibly small as long as the negatively charged HCO_3^- state is stable at Fe^{2+}.

In contrast, the bidentate-to-monodentate reorientation is slightly uphill in $Q_A/Q_A^{\cdot-}$, as the monodentate bicarbonate can accept an H-bond from D1-Tyr246 (**Figures 3B,C**). Note that $Q_A^{\cdot-}$ is stabilized when the hydroxyl group of D1-Tyr246 is oriented toward $Q_A^{\cdot-}$ (Saito et al., 2013). It has been proposed that bicarbonate serves as not only a bidentate but also a monodentate ligand (Hienerwadel and Berthomieu, 1995; Chernev et al., 2011; Uto et al., 2017). In vacuum, the monodentate ligation may become pronounced specifically upon the formation of $Q_A^{\cdot-}$ (Chernev et al., 2011), because the reorientation of the free bicarbonate ligand occurs easily and is the only way to compensate for the electrostatic repulsion against $Q_A^{\cdot-}$. The corresponding electrostatic repulsion is smaller (bicarbonate...$Q_A^{\cdot-}$ = 6.8 Å) than the interactions with D1-Glu244 (3.4 Å from bicarbonate), D1-Tyr246 (3.2 Å), and D2-Tyr244 (3.1 Å) in the PSII protein environment. The shape of the potential-energy profile remains essentially unaffected in response to changes in the Q_A redox state (**Figures 3B,C**). Furthermore, the bidentate

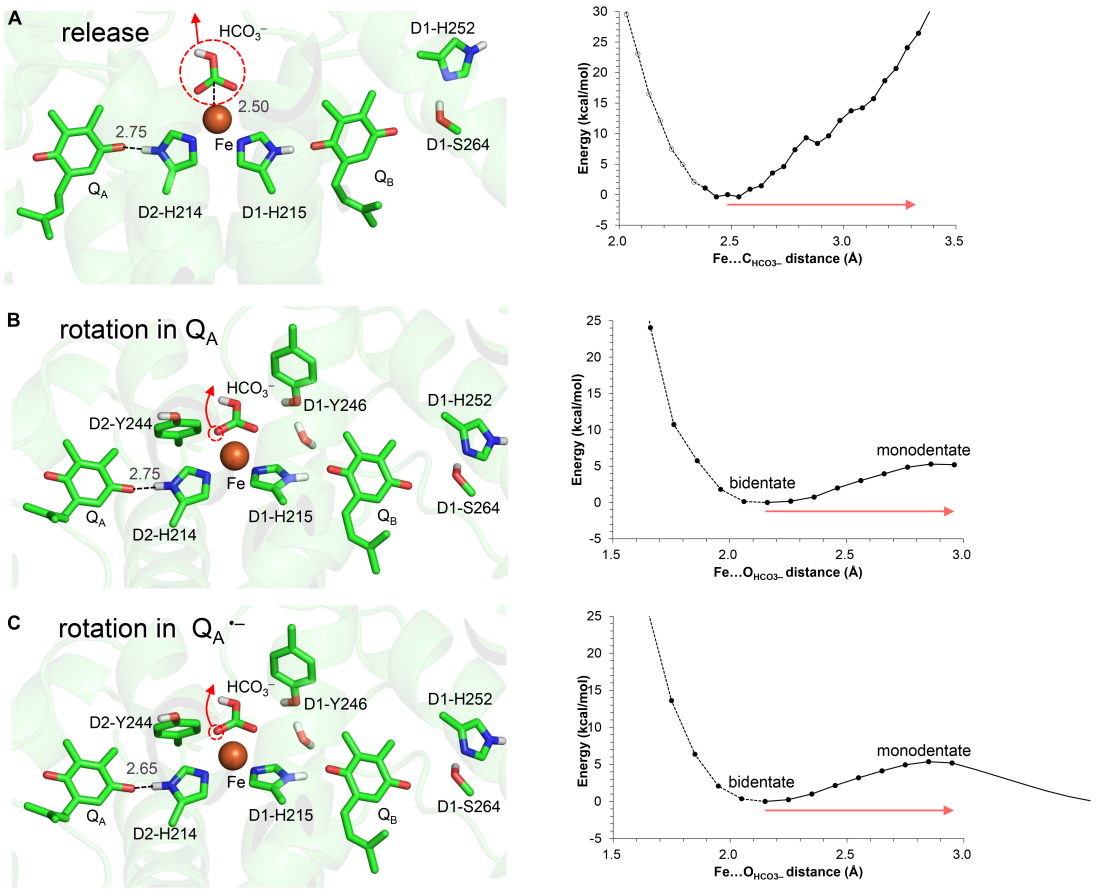

FIGURE 3
Energy profile for the bicarbonate displacement. **(A)** Release of the bicarbonate ligand from the Fe^{2+} site. **(B)** Bidentate-to-monodentate reorientation of the bicarbonate ligand in neutral Q_A. **(C)** Bidentate-to-monodentate reorientation of the bicarbonate ligand in $Q_A^{\bullet-}$. Red arrows indicate the orientations of the bicarbonate displacement. Note that the geometry of each intermediate conformation is fully QM/MM optimized.

ligation is more stable than the monodentate ligation in the PSII protein environment (**Figures 3B,C**). Thus, the bidentate-to-monodentate reorientation is unlikely to synchronize with unimpaired electron transfer from Q_A to Q_B: the reorientation may occur only when the electron transfer is sufficiently slow to compete with the energetically uphill movement of the bicarbonate ligand.

These results suggest that the release of the bicarbonate ligand is energetically more uphill than the reorientation, as long as HCO_3^- is ligated to the Fe^{2+} site.

Discussion

Possible mechanisms of bicarbonate loss

The bicarbonate protonation and decomposition can also lead to the bicarbonate loss (e.g., Loerting et al., 2000). This requires the proton transfer pathway toward the bicarbonate binding site. Below we have discussed candidate proton-donor residues near the bicarbonate binding site.

Notably, the bicarbonate binding site is linked with the protein bulk surface *via* an H-bond network that is formed by D1-Glu244, D1-Tyr246, and D1-Ser264 (**Figure 4**). D1-Glu244 in the highly charged *de*-loop region was responsible for the pH dependence of E_m for the non-heme Fe complex (Ishikita and Knapp, 2005b) and may be involved in the bicarbonate protonation at lower pH in the Fe^{2+} state (Kato et al., 2021). In addition, the $E_m(Q_A)$ shift was observed upon the D1-E244A mutation (Forsman et al., 2019). Indeed, D1-Glu244 is close to the bicarbonate (3.37 Å, **Figure 1**) (Umena et al., 2011). However, according to the geometry of the PSII crystal structure, ionized D1-Glu244 is stabilized by a salt bridge with D2-Lys264 (3.31 Å, Umena et al., 2011) and is unlikely to serve as a proton donor to the bicarbonate. Unless structural changes occur at higher pH, the geometry does not directly support the involvement of D1-Glu244 in the bicarbonate protonation.

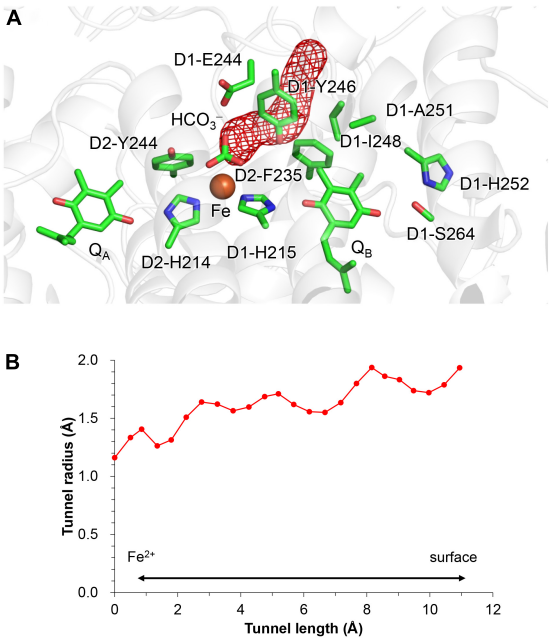

FIGURE 4
Channel that proceeds from the bicarbonate binding site toward the stromal protein surface. **(A)** Overview of the hydrophobic channel (red mesh). **(B)** Cavity radius along the hydrophobic channel. The channel space was analyzed using CAVER (Chovancova et al., 2012).

Although D1-Ser268 does not form an H-bond with the bicarbonate ligand (4.57 Å, Umena et al., 2011), the existence of a water molecule, which is only 2.44 Å away from the D1-Ser268 side chain (2.44 Å, Umena et al., 2011), is remarkable. The short distance might be due to the water molecule being H_3O^+ [e.g., O. . .O = 2.4 Å for typical H_2O. . .H_3O^+ (Mikenda, 1986; Limbach et al., 2009; **Figure 1A**)]. However, assuming that the water molecule is H_3O^+ in the QM/MM calculation, H_3O^+ forms H-bonds with D1-Tyr246 and a water molecule adjacent to D1-Glu244, but not with D1-Ser268; this increases the $O_{D1-Ser268}$. . .O_{H3O+} distance to 2.98 Å (**Figure 5**). Furthermore, H_3O^+ is unstable at this site, releasing the proton to ionized D1-Glu244. H_3O^+ can exist at the D1-Ser268 moiety only when D1-Glu244 is protonated. However, proton transfer from H_3O^+ at the D1-Ser268 to the bicarbonate ligand is energetically uphill (**Figure 5**), which suggests that D1-Ser268 is unlikely the proton donor to the bicarbonate. D1-Ser268 and the adjacent water molecule may be more likely to be involved in the proton transfer associated with the Q_BH_2 release, as suggested for mutant PSII proteins (Forsman and Eaton-Rye, 2020).

D1-Tyr246 does not form an H-bond with the bicarbonate –OH group (3.80 Å) in the PSII crystal structure (Umena et al., 2011), whereas D1-Tyr246 forms an H-bond with the bicarbonate –OH group (≈2.7 Å) in response to the bidentate-to-monodentate reorientation according to QM/MM calculations (**Figure 3**). D1-Tyr246 is located at the unique position, the interface between the channel that proceeds from the bicarbonate binding site (**Figure 4**) and the inner cavity, the Q_B pocket.

The elongation electron density near the hydroxyl group of D1-Tyr246 (Saito et al., 2013) may be interpreted as a peroxide O with the O–O distance of 1.48 Å, which can be fitted to the density (**Figure 1A**; Saito et al., 2013). Although the peroxide O is oriented toward the Q_B binding pocket, the link between the bicarbonate binding site and the Q_B binding pocket *via* D1-Tyr246 is weak due to the less polar O site.

Alternatively, the elongation of the density may be interpreted as H_3O^+. In the crystal structure reported by Uto et al. (2017), the $O_{D1-Tyr246}$. . .O_{water} distance of 2.3 Å is closer to the O. . .O distance for a typical Zundel (H_2O. . .H^+. . .H_2O) cation (≈2.3 Å), which suggests that the density may originate from H_3O^+ (**Figure 1B**). In this case, the H^+ needs to enter *via* the Q_B-exchange channel, possibly during the Q_B exchange.

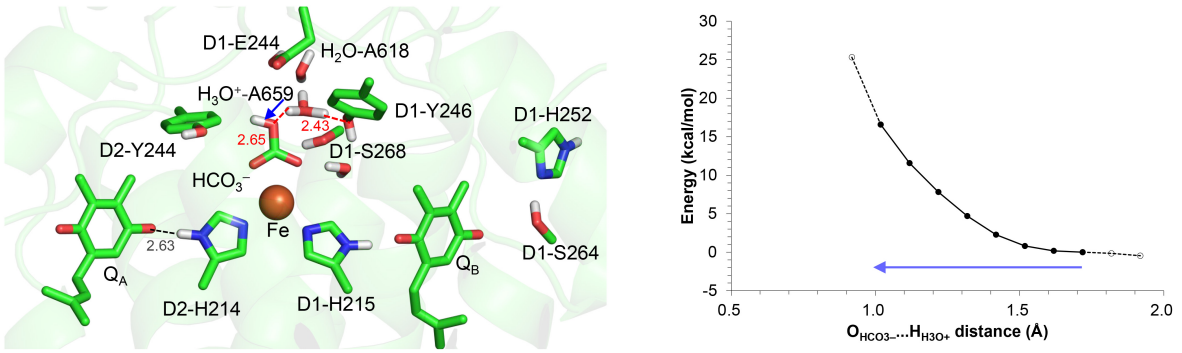

FIGURE 5
Potential energy profile for proton transfer from H_3O^+ at D1-Ser268 to the bicarbonate ligand. The blue arrow indicates the orientation of the proton transfer. Note that the geometry of each intermediate conformation is fully QM/MM optimized.

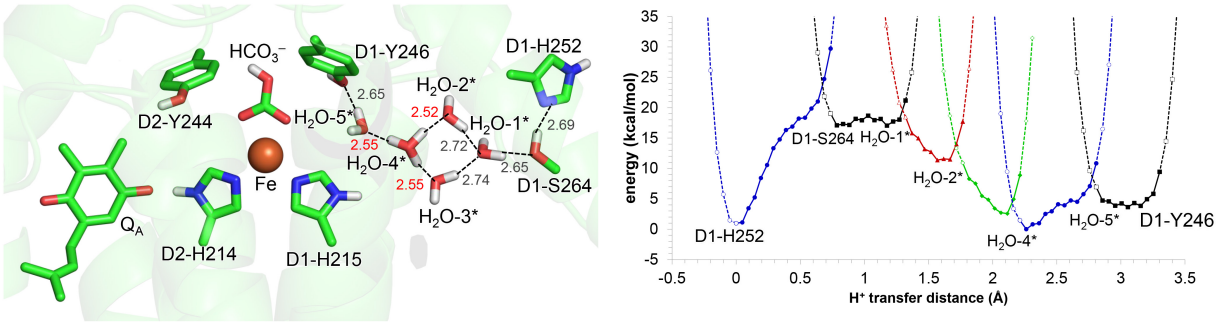

FIGURE 6
Potential energy profile for proton transfer in the Q_B binding pocket, adding water molecules (*: H_2O-1 to 5). Note that the geometry of each intermediate conformation is fully QM/MM optimized.

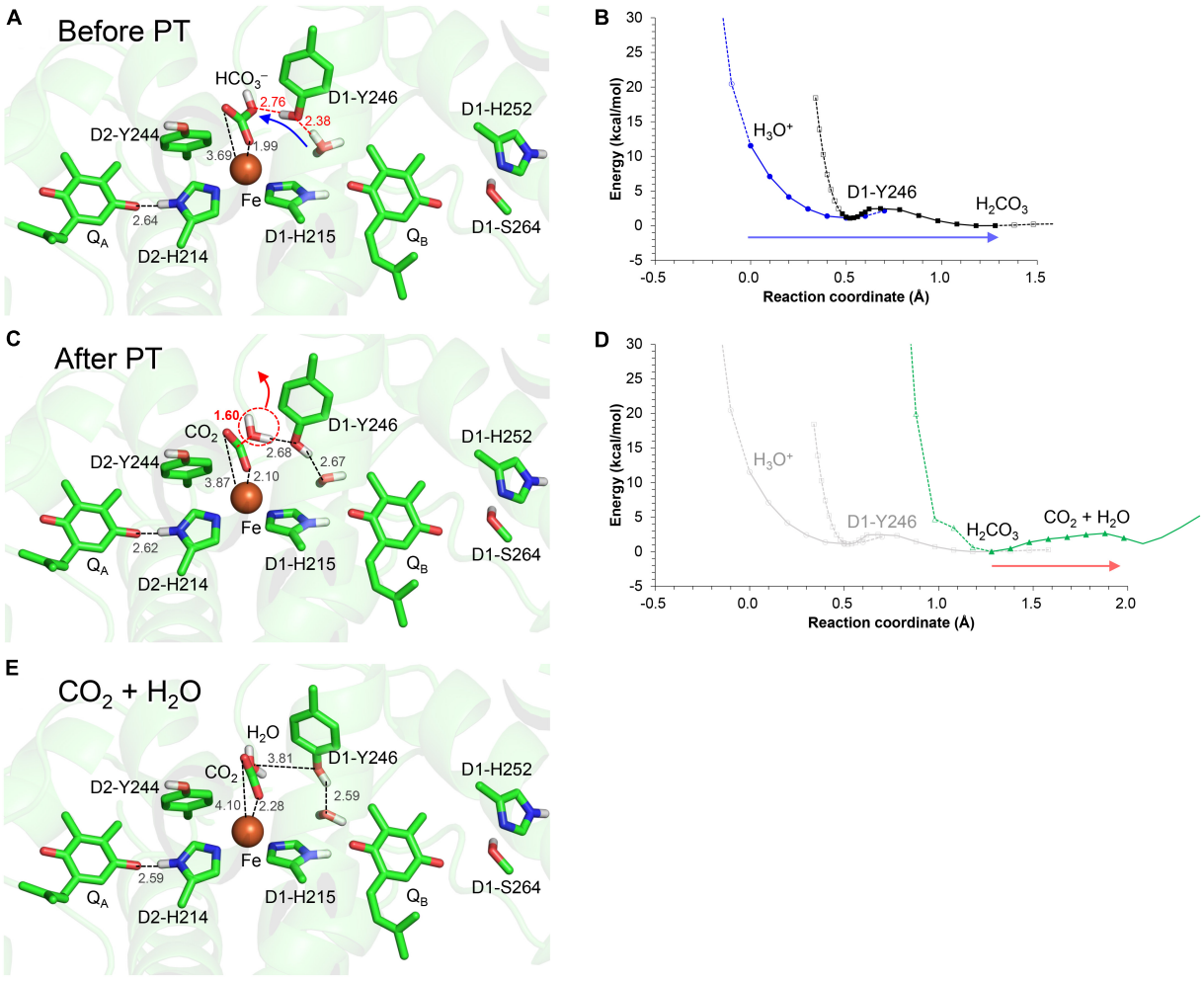

FIGURE 7
H-bond network *via* D1-Tyr246 to the monodentate bicarbonate ligand. **(A)** QM/MM-optimized geometry before proton transfer. **(B)** Potential energy profile for proton transfer along the H_3O^+. . .D1-Tyr246. . .bicarbonate H-bond network. **(C)** QM/MM-optimized geometry after proton transfer. **(D)** Potential energy profile for CO_2 release from the monodentate binding site. **(E)** QM/MM-optimized geometry after decomposition to H_2O and CO_2. Blue arrows indicate the orientations of the proton transfer. Red arrows indicate the orientations of the structural changes. Note that the geometry of each intermediate conformation is fully QM/MM optimized.

To investigate whether the uptake and existence of the H^+ are energetically possible in the Q_B binding pocket, QM/MM calculations were performed, removing Q_B and filling the pocket with water molecules. The potential-energy profile indicates that the proton is energetically stable and populated among the two water molecules that bridge between D1-His215 and D1-Tyr246 (i.e., H_2O-4* and H_2O-5*), as H_3O^+ is stabilized by three H-bond acceptor groups (**Figure 6**). After Q_B re-enters the binding pocket, the H^+ is allowed to exist only at the non-excluded water molecules, e.g., the one adjacent to D1-Tyr246. Indeed, the bulky methoxy groups of ubiquinone in PbRC are replaced with the methyl groups of plastoquinone in PSII, allowing one water molecules to remain at the D1-Tyr246 moiety. Thus, a water molecule can remain at the D1-Tyr246 moiety, the only polar site in the bottleneck of the hydrophobic Q_B pocket. This is likely the cause of the elongation of the electron density adjacent to the –OH region of D1-Tyr246.

When H_3O^+ is adjacent to D1-Tyr246, the bidentate-to-monodentate reorientation leads to the formation of an H-bond network that proceeds from H_3O^+ *via* D1-Tyr246 toward the monodentate bicarbonate (**Figure 7A**). The potential energy profile for the H-bonds suggests that the H-bond network can serve as a proton-transfer pathway (**Figure 7B**).

Intriguingly, when the proton arrives at the bicarbonate moiety along the Grotthuss-like proton conduit, the bicarbonate undergoes protonation (**Figure 7C**) followed by conversion to H_2O and CO_2 (**Figure 7D**). As the products move away from the Fe^{2+} site, the shape of O...C...O becomes linear, i.e., O = C = O (**Figure 7E**). Thus, the bicarbonate loss can occur through the conversion of the protonated bicarbonate to CO_2 and H_2O at the Fe^{2+} moiety (**Figure 7D**), which is in line with the CO_2 release observed on the electron-acceptor side (Shevela et al., 2020).

The bidentate-to-monodentate reorientation of the bicarbonate ligand is a low-barrier process (**Figure 3**). In the monodentate bicarbonate ligand, the H_3O^+...D1-Tyr246...$HCO_3^-/Q_A^{\cdot -}$ H-bond network is formed. The hydroxyl group forms a Grotthuss-like proton transfer pathway, accepting the proton from H_3O^+ and donating it to the bicarbonate. That is, D1-Tyr246 remains protonated during proton transfer, as suggested using Fourier transform infrared (FTIR) spectroscopy (Takahashi et al., 2009). The absence of the proton donor (H_3O^+), proton-conducting side chain (D1-Tyr246), and decomposable carboxylic ligand (bicarbonate) in PbRC implies that the proton-mediated $Q_A^{\cdot -}$ stabilization occurs specifically in O_2-evolving PSII for photoprotection. The involvement of D1-Tyr246 in the photoprotective role (proton-mediated $Q_A^{\cdot -}$ stabilization) is in line with the findings of mutational studies; the photoautotrophic growth was slower in the D1-Y246F mutant PSII than in wild-type PSII (Kless et al., 1994); the D1-Y246A mutant PSII was also unable to grow photoautotrophically under strong light (Forsman et al., 2019).

The polar –OH region of D1-Tyr246 on the surface of the Q_B binding pocket can mediate the conduction of the proton to the bicarbonate binding site. The low-barrier bidentate-to-monodentate reorientation contributes to the formation of the "proton wire" (Stuchebrukhov, 2009) between D1-Tyr246 and the unligated –OH site of the bicarbonate. The corresponding H-bond formation with D1-Tyr246 does not occur upon the replacement of bicarbonate with formate, because formate has no –OH site. The absence of the –OH site may also be an origin of why formate substitution inhibits electron transfer from Q_A to Q_B (Eaton-Rye and Govindjee, 1988) or the exchange of Q_BH_2 (Sedoud et al., 2011). Thus, the hydrophobic and pre-organized protein electrostatic environment (Warshel, 1998; Warshel et al., 2006) on the bicarbonate binding site is likely to reduce the energy barrier for the bicarbonate protonation with respect to the bulk region, facilitating the direct protonation of the –OH site of the bicarbonate and the release of the product, gaseous CO_2, without the formation of the typical $(HO)_2C = O$ intermediate (Loerting et al., 2000).

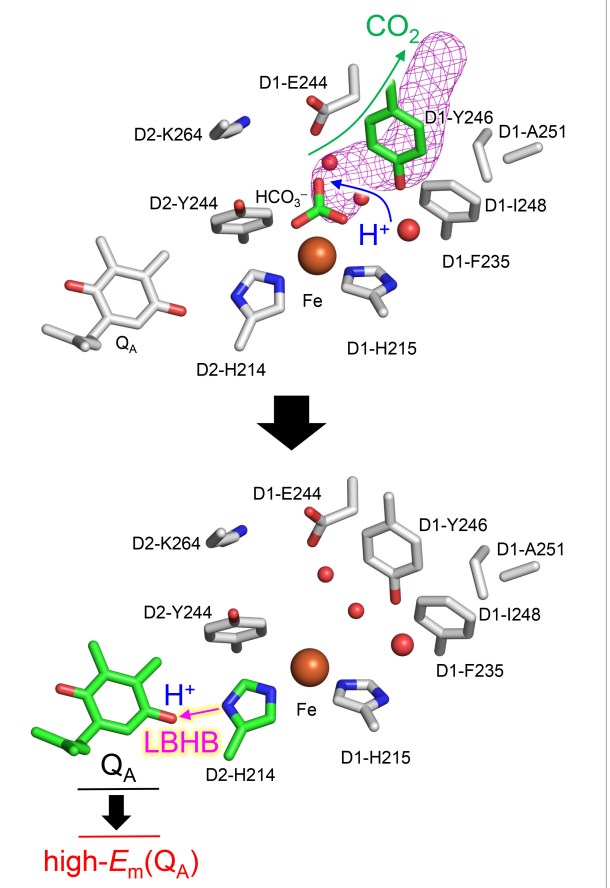

FIGURE 8
Overview of the proton-mediated photoprotection mechanism in photosystem II.

Molecular dynamics simulations suggested that the polar –OH site of the bicarbonate is linked to water molecules in the Q_B binding pocket *via* D1-Tyr246 during Q_BH_2 release (Sugo et al., 2022). These water molecules serve as a proton transfer pathway for the reprotonation of D1-His215 (Sugo et al., 2022), the proton donor during Q_BH^-/Q_BH_2 conversion (Saito et al., 2013, 2020). Thus, the link between the polar –OH site and D1-Tyr246 may provide a key to understand how the bicarbonate is associated with Q_BH_2 release, interacting with water molecules in the reprotonation pathway for D1-His215.

Hydrophobic residues that form a CO_2-releasing channel

QM/MM calculations suggest that the product, CO_2, enters the channel that proceeds *via* D1-Glu244 and D1-Tyr246 toward the stromal protein surface (**Figure 4**). The entrance of the channel is hydrophobic, being formed by the side chains of D1-Tyr246, D2-Phe235, and D1-Ile248.

D1-Tyr246 may play two roles in the protonation of bicarbonate. While the polar –OH region mediates the conduction of the proton to the bicarbonate protonation site, the hydrophobic ring region can isolate the bicarbonate from the water molecules in the Q_B binding pocket, making the bicarbonate binding moiety hydrophobic. The loss of the solvation also increases $pK_a(HCO_3^-/H_2CO_3)$ with respect to the bulk water region, facilitating the conversion of bicarbonate to gaseous CO_2.

Conclusion

In response to the loss of the bicarbonate ligand, a short low-barrier H-bond forms between D2-His214 and $Q_A^{\cdot -}$, which facilitates the proton migration toward $Q_A^{\cdot -}$ and increases $E_m(Q_A)$ (**Figure 2**). The loss of bicarbonate may be induced by the protonation. The D1-Glu244 conformation identified in the PSII crystal structure does not support the role in donating a proton to the bicarbonate ligand, whereas D1-Tyr246 may facilitate bicarbonate protonation and decomposition into H_2O and CO_2 (**Figure 7**). The channel, which is formed by D1-Tyr246, D2-Phe235, and D1-Ile248, may serve as a CO_2-releasing channel (**Figure 4**). These constitute the basis for the photoprotection mechanism through the high-$E_m(Q_A)$ conformation, which inhibits the backward electron transfer from $Q_A^{\cdot -}$ *via* the triplet-generating pheophytin/chlorophyll cofactors (**Figure 7**). The proton-mediated photoprotection mechanism is pronounced exclusively in PSII, as the bicarbonate ligand is replaced with Glu-M234 in PbRC from *Rhodobacter sphaeroides* (**Figure 8**). The mechanism of the low-barrier H-bond formation caused by the loss of the bicarbonate ligand may also be associated with the Q_AH_2 formation under high light in PSII (Vass et al., 1992; Noguchi, 2002), as Glu-M234 exists permanently and Q_A never leaves in PbRC (Wei et al., 2022). These findings could elucidate how the type-II reaction centers show notable structural differences not only on the lumenal oxygen-evolving side but also on the stromal electron acceptor side.

Data availability statement

The original contributions presented in this study are included in the article/**Supplementary material**, further inquiries can be directed to the corresponding author.

Author contributions

HI designed the research and wrote the manuscript. YS and HI performed the research and analyzed the data. Both authors contributed to the article and approved the submitted version.

Funding

This research was supported by JST CREST (JPMJCR1656 to HI), JSPS KAKENHI (JP18H01937, JP18H05155, JP20H03217, and JP20H05090 to HI), and Interdisciplinary Computational Science Program in CCS, University of Tsukuba.

Conflict of interest

The authors declare that the research was conducted in the absence of any commercial or financial relationships that could be construed as a potential conflict of interest.

Publisher's note

Supplementary material

The Supplementary Material for this article can be found online at: https://www.frontiersin.org/articles/10.3389/fpls.2022.934736/full#supplementary-material

References

Ashizawa, R., and Noguchi, T. (2014). Effects of hydrogen bonding interactions on the redox potential and molecular vibrations of plastoquinone as studied using density functional theory calculations. *Phys. Chem. Chem. Phys.* 16, 11864–11876. doi: 10.1039/c3cp54742f

Brinkert, K., De Causmaecker, S., Krieger-Liszkay, A., Fantuzzi, A., and Rutherford, A. W. (2016). Bicarbonate-induced redox tuning in Photosystem II for regulation and protection. *Proc. Natl. Acad. Sci. U.S.A.* 113, 12144–12149. doi: 10.1073/pnas.1608862113

Brooks, B. R., Bruccoleri, R. E., Olafson, B. D., States, D. J., Swaminathan, S., and Karplus, M. (1983). CHARMM: a program for macromolecular energy, minimization, and dynamics calculations. *J. Comput. Chem.* 4, 187–217. doi: 10.1002/jcc.540040211

Chernev, P., Zaharieva, I., Dau, H., and Haumann, M. (2011). Carboxylate shifts steer interquinone electron transfer in photosynthesis. *J. Biol. Chem.* 286, 5368–5374. doi: 10.1074/jbc.M110.202879

Chovancova, E., Pavelka, A., Benes, P., Strnad, O., Brezovsky, J., Kozlikova, B., et al. (2012). CAVER 3.0: a tool for the analysis of transport pathways in dynamic protein structures. *PLoS Comput. Biol.* 8:e1002708. doi: 10.1371/journal.pcbi.1002708

De Causmaecker, S., Douglass, J. S., Fantuzzi, A., Nitschke, W., and Rutherford, A. W. (2019). Energetics of the exchangeable quinone Q_B in photosystem II. *Proc. Natl. Acad. Sci. U.S.A.* 116, 19458–19463. doi: 10.1073/pnas.1910675116

Diner, B. A., and Petrouleas, V. (1987). Q_{400}, the non-heme iron of the photosystem II iron-quinone complex. A spectroscopic probe of quinone and inhibitor binding to the reaction center. *Biochim. Biophys. Acta* 895, 107–125. doi: 10.1016/S0304-4173(87)80010-1

Eaton-Rye, J. J., and Govindjee. (1988). Electron transfer through the quinone acceptor complex of photosystem II after one or two actinic flashes in bicarbonate-depleted spinach thylakoid membranes. *Biochim. Biophys. Acta* 935, 248–257. doi: 10.1016/0005-2728(88)90221-6

Ferreira, K. N., Iverson, T. M., Maghlaoui, K., Barber, J., and Iwata, S. (2004). Architecture of the photosynthetic oxygen-evolving center. *Science* 303, 1831–1838. doi: 10.1126/science.1093087

Forsman, J. A., and Eaton-Rye, J. J. (2020). The D1:Ser268 residue of Photosystem II contributes to an alternative pathway for Q_B protonation in the absence of bound bicarbonate. *FEBS Lett.* 594, 2953–2964. doi: 10.1002/1873-3468.13880

Forsman, J. A., Vass, I., and Eaton-Rye, J. J. (2019). D1:Glu244 and D1:Tyr246 of the bicarbonate-binding environment of Photosystem II moderate high light susceptibility and electron transfer through the quinone-Fe-acceptor complex. *Biochim. Biophys. Acta* 1860:148054. doi: 10.1016/j.bbabio.2019.07.009

Gisriel, C. J., Wang, J., Liu, J., Flesher, D. A., Reiss, K. M., Huang, H.-L., et al. (2022). High-resolution cryo-electron microscopy structure of photosystem II from the mesophilic cyanobacterium, *Synechocystis* sp. PCC 6803. *Proc. Natl. Acad. Sci. U.S.A.* 119:e2116765118. doi: 10.1073/pnas.2116765118

Grimsley, G. R., Scholtz, J. M., and Pace, C. N. (2009). A summary of the measured p*K* values of the ionizable groups in folded proteins. *Protein Sci.* 18, 247–251. doi: 10.1002/pro.19

Hasegawa, R., Saito, K., Takaoka, T., and Ishikita, H. (2017). pK_a of ubiquinone, menaquinone, phylloquinone, plastoquinone, and rhodoquinone in aqueous solution. *Photosynth. Res.* 133, 297–304. doi: 10.1007/s11120-017-0382-y

Hay, P. J., and Wadt, W. R. (1985). *Ab initio* effective core potentials for molecular calculations. Potentials for K to Au including the outermost core orbitals. *J. Chem. Phys.* 82, 299–310. doi: 10.1063/1.448975

Hienerwadel, R., and Berthomieu, C. (1995). Bicarbonate binding to the non-heme iron of photosystem II investigated by Fourier transform infrared difference spectroscopy and ^{13}C-labeled bicarbonate. *Biochemistry* 34, 16288–16297. doi: 10.1021/bi00050a008

Hsueh, K. L., Westler, W. M., and Markley, J. L. (2010). NMR investigations of the Rieske protein from *Thermus thermophilus* support a coupled proton and electron transfer mechanism. *J. Am. Chem. Soc.* 132, 7908–7918. doi: 10.1021/ja1026387

Ishikita, H., and Knapp, E.-W. (2005a). Control of quinone redox potentials in photosystem II: electron transfer and photoprotection. *J. Am. Chem. Soc.* 127, 14714–14720. doi: 10.1021/ja052567r

Ishikita, H., and Knapp, E.-W. (2005b). Oxidation of the non-heme iron complex in photosystem II. *Biochemistry* 44, 14772–14783. doi: 10.1021/bi051099v

Ishikita, H., and Saito, K. (2014). Proton transfer reactions and hydrogen-bond networks in protein environments. *J. R. Soc. Interface* 11:20130518. doi: 10.1098/rsif.2013.0518

Johnson, G. N., Rutherford, A. W., and Krieger, A. (1995). A change in the midpoint potential of the quinone Q_A in Photosystem II associated with photoactivation of oxygen evolution. *Biochim. Biophys. Acta* 1229, 202–207. doi: 10.1016/0005-2728(95)00003-2

Jursinic, P., Warden, J., and Govindjee. (1976). A major site of bicarbonate effect in system II reaction. Evidence from ESR signal II_{vf}, fast fluorescence yield changes and delayed light emission. *Biochim. Biophys. Acta* 440, 322–330. doi: 10.1016/0005-2728(76)90066-9

Kato, Y., Nagao, R., and Noguchi, T. (2016). Redox potential of the terminal quinone electron acceptor Q_B in photosystem II reveals the mechanism of electron transfer regulation. *Proc. Natl. Acad. Sci. U.S.A.* 113, 620–625. doi: 10.1073/pnas.1520211113

Kato, Y., Watanabe, H., and Noguchi, T. (2021). ATR-FTIR spectroelectrochemical study on the mechanism of the pH dependence of the redox potential of the non-heme iron in photosystem II. *Biochemistry* 60, 2170–2178. doi: 10.1021/acs.biochem.1c00341

Kimura, M., Kato, Y., and Noguchi, T. (2020). Protonation state of a key histidine ligand in the iron–quinone complex of photosystem II as revealed by light-induced ATR-FTIR spectroscopy. *Biochemistry* 59, 4336–4343. doi: 10.1021/acs.biochem.0c00810

Kless, H., Oren-Shamir, M., Malkin, S., McIntosh, L., and Edelman, M. (1994). The *D-E* region of the D1 protein is involved in multiple quinone and herbicide interactions in photosystem II. *Biochemistry* 33, 10501–10507. doi: 10.1021/bi00200a035

Krieger, A., and Weis, E. (1992). Energy dependent quenching of chlorophyll *a* fluorescence: the involvement of proton-calcium exchange at photosystem II. *Photosynthetica* 27, 89–98.

Krieger, A., Rutherford, A. W., and Johnson, G. N. (1995). On the determination of redox midpoint potential of the primary quinone electron acceptor, Q_A, in photosystem II. *Biochim. Biophys. Acta* 1229, 193–201. doi: 10.1016/0005-2728(95)00002-Z

Limbach, H.-H., Tolstoy, P. M., Pérez-Hernández, N., Guo, J., Shenderovich, I. G., and Denisov, G. S. (2009). OHO hydrogen bond geometries and NMR chemical shifts: from equilibrium structures to geometric H/D isotope effects, with applications for water, protonated water, and compressed ice. *Isr. J. Chem.* 49, 199–216. doi: 10.1560/IJC.49.2.199

Loerting, T., Tautermann, C., Kroemer, R. T., Kohl, I., Hallbrucker, A., Mayer, E., et al. (2000). On the surprising kinetic stability of carbonic acid (H_2CO_3). *Angew. Chem. Int. Ed.* 39, 891–894. doi: 10.1002/(sici)1521-3773(20000303)39:5<891::aid-anie891>3.0.co;2-e

MacKerell, A. D. Jr., Bashford, D., Bellott, R. L., Dunbrack, R. L. Jr., Evanseck, J. D., Field, M. J., et al. (1998). All-atom empirical potential for molecular modeling and dynamics studies of proteins. *J. Phys. Chem. B* 102, 3586–3616. doi: 10.1021/jp973084f

Mikenda, W. (1986). Stretching frequency versus bond distance correlation of O-D(H)$\cdots$Y (Y = N, O, S, Se, Cl, Br, I) hydrogen bonds in solid hydrates. *J. Mol. Struct.* 147, 1–15. doi: 10.1016/0022-2860(86)87054-5

Muh, F., Glockner, C., Hellmich, J., and Zouni, A. (2012). Light-induced quinone reduction in photosystem II. *Biochim. Biophys. Acta* 1817, 44–65. doi: 10.1016/j.bbabio.2011.05.021

Nakamura, S., and Noguchi, T. (2017). Infrared determination of the protonation state of a key histidine residue in the photosynthetic water oxidizing center. *J. Am. Chem. Soc.* 139, 9364–9375. doi: 10.1021/jacs.7b04924

Noguchi, T. (2002). Dual role of triplet localization on the accessory chlorophyll in the photosystem II reaction center: photoprotection and photodamage of the D1 protein. *Plant Cell Physiol.* 43, 1112–1116. doi: 10.1093/pcp/pcf137

QSite (2012). *version 5.8*. New York, NY: Schrödinger LLC.

Rutherford, A. W., and Krieger-Liszkay, A. (2001). Herbicide-induced oxidative stress in photosystem II. *Trends Biochem. Sci.* 26, 648–653. doi: 10.1016/s0968-0004(01)01953-3

Rutherford, A. W., Osyczka, A., and Rappaport, F. (2012). Back-reactions, short-circuits, leaks and other energy wasteful reactions in biological electron transfer: redox tuning to survive life in O_2. *FEBS Lett.* 586, 603–616. doi: 10.1016/j.febslet.2011.12.039

Saito, K., Mandal, M., and Ishikita, H. (2020). Redox potentials along the redox-active low-barrier H-bonds in electron transfer pathways. *Phys. Chem. Chem. Phys.* 22, 25467–25473. doi: 10.1039/d0cp04265j

Saito, K., Rutherford, A. W., and Ishikita, H. (2013). Mechanism of proton-coupled quinone reduction in Photosystem II. *Proc. Natl. Acad. Sci. U.S.A.* 110, 954–959. doi: 10.1073/pnas.1212957110

Saito, K., Rutherford, A. W., and Ishikita, H. (2015). Energetics of proton release on the first oxidation step in the water-oxidizing enzyme. *Nat. Commun.* 6:8488. doi: 10.1038/ncomms9488

Sedoud, A., Kastner, L., Cox, N., El-Alaoui, S., Kirilovsky, D., and Rutherford, A. W. (2011). Effects of formate binding on the quinone-iron electron acceptor complex of photosystem II. *Biochim. Biophys. Acta* 1807, 216–226. doi: 10.1016/j.bbabio.2010.10.019

Shen, J. R. (2015). The structure of photosystem II and the mechanism of water oxidation in photosynthesis. *Annu. Rev. Plant. Biol.* 66, 23–48. doi: 10.1146/annurev-arplant-050312-120129

Shevela, D., Do, H.-N., Fantuzzi, A., Rutherford, A. W., and Messinger, J. (2020). Bicarbonate-mediated CO_2 formation on both sides of photosystem II. *Biochemistry* 59, 2442–2449. doi: 10.1021/acs.biochem.0c00208

Shevela, D., Eaton-Rye, J. J., Shen, J. R., and Govindjee. (2012). Photosystem II and the unique role of bicarbonate: a historical perspective. *Biochim. Biophys. Acta* 1817, 1134–1151. doi: 10.1016/j.bbabio.2012.04.003

Shibamoto, T., Kato, Y., Sugiura, M., and Watanabe, T. (2009). Redox potential of the primary plastoquinone electron acceptor Q_A in photosystem II from *Thermosynechococcus elongatus* determined by spectroelectrochemistry. *Biochemistry* 48, 10682–10684. doi: 10.1021/bi901691j

Siggel, U., Khanna, R., Renger, G., and Govindjee. (1977). Investigation of the absorption changes of the plasto-quinone system in broken chloroplasts. The effect of bicarbonate-depletion. *Biochim. Biophys. Acta* 462, 196–207. doi: 10.1016/0005-2728(77)90202-x

Stuchebrukhov, A. A. (2009). Mechanisms of proton transfer in proteins: localized charge transfer versus delocalized soliton transfer. *Phys. Rev. E Stat. Nonlin. Soft Matter Phys.* 79:031927. doi: 10.1103/PhysRevE.79.031927

Suga, M., Akita, F., Hirata, K., Ueno, G., Murakami, H., Nakajima, Y., et al. (2015). Native structure of photosystem II at 1.95 Å resolution viewed by femtosecond X-ray pulses. *Nature* 517, 99–103. doi: 10.1038/nature13991

Sugo, Y., Saito, K., and Ishikita, H. (2021). Mechanism of the formation of proton transfer pathways in photosynthetic reaction centers. *Proc. Natl. Acad. Sci. U.S.A.* 118:e2103203118.

Sugo, Y., Saito, K., and Ishikita, H. (2022). Conformational changes and H-bond rearrangements during quinone release in photosystem II. *Biochemistry* doi: 10.1021/acs.biochem.1022c00324

Takahashi, R., Boussac, A., Sugiura, M., and Noguchi, T. (2009). Structural coupling of a tyrosine side chain with the non-heme iron center in photosystem II as revealed by light-induced Fourier transform infrared difference spectroscopy. *Biochemistry* 48, 8994–9001. doi: 10.1021/bi901195e

Umena, Y., Kawakami, K., Shen, J.-R., and Kamiya, N. (2011). Crystal structure of oxygen-evolving photosystem II at a resolution of 1.9 Å. *Nature* 473, 55–60.

Uto, S., Kawakami, K., Umena, Y., Iwai, M., Ikeuchi, M., Shen, J. R., et al. (2017). Mutual relationships between structural and functional changes in a PsbM-deletion mutant of photosystem II. *Faraday Discuss* 198, 107–120. doi: 10.1039/c6fd00213g

Vacek, G., Perry, J. K., and Langlois, J. M. (1999). Advanced initial-guess algorithm for self-consistent-field calculations on organometallic systems. *Chem. Phys. Lett.* 310, 189–194.

Vass, I., Styring, S., Hundal, T., Koivuniemi, A., Aro, E. M., and Andersson, B. (1992). Reversible and irreversible intermediates during photoinhibition of photosystem II: stable reduced Q_A species promote chlorophyll triplet formation. *Proc. Natl. Acad. Sci. U.S.A.* 89, 1408–1412. doi: 10.1073/pnas.89.4.1408

Warshel, A. (1998). Electrostatic origin of the catalytic power of enzymes and the role of preorganized active sites. *J. Biol. Chem.* 273, 27035–27038. doi: 10.1074/jbc.273.42.27035

Warshel, A., Sharma, P. K., Kato, M., and Parson, W. W. (2006). Modeling electrostatic effects in proteins. *Biochim. Biophys. Acta* 1764, 1647–1676.

Wei, R. J., Zhang, Y., Mao, J., Kaur, D., Khaniya, U., and Gunner, M. R. (2022). Comparison of proton transfer paths to the Q_A and Q_B sites of the *Rb. sphaeroides* photosynthetic reaction centers. *Photosynth. Res.* doi: 10.1007/s11120-11022-00906-x

Zu, Y., Couture, M. M., Kolling, D. R., Crofts, A. R., Eltis, L. D., Fee, J. A., et al. (2003). Reduction potentials of Rieske clusters: importance of the coupling between oxidation state and histidine protonation state. *Biochemistry* 42, 12400–12408. doi: 10.1021/bi0350957